# FLOW MODELING IN A SHELL AND TUBE HEAT EXCHANGER WITHOUT PHASE CHANGE

*A Thesis Submitted*
In Partial Fulfilment of the Requirements
for the Degree of
MASTER OF TECHNOLOGY

*by*

SANJAY R. DESHPANDE

*to the*

DEPARTMENT OF MECHANICAL ENGINEERING
**INDIAN INSTITUTE OF TECHNOLOGY, KANPUR**
APRIL, 1987

CENTRAL LIBRARY
Acc. No. A 92334

Thesis
621.4022

ME- 1987-M- DES-FLO

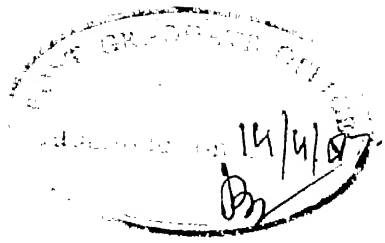

CERTIFICATE

This is to certify that the work entitled 'Flow Modeling in a Shell and Tube Heat Exchanger Without Phase Change', has been carried out by Sanjay R. Deshpande under our supervision and has not been submitted elsewhere for the award of a degree.


Dr. M.S. Kalra
Assistant Professor
Department of Mechanical Engg.
Indian Institute of Technology,
Kanpur, India-208016

Dr. Keshav Kant
Assistant Professor
Department of Mech. Engg.
Indian Institute of Techn
Kanpur, India-208016


April 1987

## ACKNOWLEDGEMENTS

I take this opportunity to express my profound gratitude to my thesis supervisors Dr. Keshav Kant and Dr. M.S. Kalra for their kind help, guidance and moral support throughout the project.

I would also like to thank all my friends who have made my stay at I.I.T. Kanpur a memorable one.

I would like to thank Mr. H.V.C. Srivastava for his excellent typing, Mr. Ananto for his excellent drawings and Mr. Lalta Prasad for his meticulous cyclostyling.

SANJAY

# CONTENTS

# LIST OF FIGURES

## LIST OF SYMBOLS

| | |
|---|---|
| A | Global fluid matrix |
| $A^e$ | Elemental area, Nondimensional |
| B | Global matrix for the mass flux at the boundary |
| $C^e$ | Elemental boundary, Non-dimensional |
| d | Tube diameter, m |
| $d_h$ | Mean hydraulic diameter on shell side, m. |
| f | friction factor for the flow over the tube bundle in the axial direction, Nondimensional. |
| $f_r$ | friction factor for the cross flow through tube bundle, Nondimensional. |
| $f_x, f_y$ | Body forces in the x and y directions respectively, $N\ m^{-3}$. |
| F | Global body force matrix |
| G | Local mass flow rate, shell-side, $kg\ s^{-1}\ m^{-2}$. |
| i,j,k,l | Node numbers for the element under consideration. |
| L | Length of heat exchanger, m. |
| m | Number of the corner nodes in the element. |
| $m_1, m_2$ | Number of Gauss points in the X and Y-directions respectively. |
| $M_i, M_l$ | Shape functions for four noded element. at $i^{th}$ and $l^{th}$ node. |

| | |
|---|---|
| $n$ | Total number of nodes in the element. |
| $N_i, N_j, N_k$ | Shape functions for eight noded element at $i^{th}, j^{th}$ and $k^{th}$ node respectively. |
| $p$ | Pressure at a point, Nondimentional |
| $p^*$ | Pressure at a point, $Nm^{-2}$ |
| $q$ | Resultant velocity at a point, $ms^{-1}$ |
| $Re_s$ | Shell-side Reynold's number. |
| $R_x, R_y$ | Resistances for the fluid flow in the x and y-directions respectively, $Nm^{-3}$. |
| $t_p$ | Tube-pitch, m. |
| $u$ | X-direction velocity, non-dimensional |
| $u^*$ | X-direction velocity, $ms^{-1}$ |
| $u_o$ | Center line velocity in the inlet pipe of heat exchanger, $ms^{-1}$. |
| $v$ | Y-direction velocity, non-dimensional |
| $v^*$ | Y-direction velocity, $ms^{-1}$ |

Greek Symbols

| | |
|---|---|
| $\lambda$ | Global matrix of unknown variables. |
| $\nu_s$ | Kinematic viscosity of shell-side fluid $m^2s^{-1}$ |
| $\varepsilon, \eta$ | Local normalised co-ordinate system for an element |
| $\Psi$ | Stream function Non-dimensional |
| $\rho_s$ | Density of shell side fluid, kg $m^{-3}$. |

## ABSTRACT

For the first time a two dimensional flow model was developed for a shell and tube heat exchanger without phase change. For the shell side fluid, the conservation equations of mass and momentum were modified using the concepts of volume porosity and distributed resistance to account for the presence of a tube bundle. The conservation equations were solved using the Finite Element Method to obtain the velocity field inside a shell and tube heat exchanger. The computational method used is capable of handling a finer mesh for a large calculation domain and it gives a faster convergence. It also makes it possible to save a lot of computer core memory and computational time. The results obtained were encouraging and showed an expected behavior.

The flexibility of the computer code developed makes it useful to model flows in many other types of heat exchangers.

# CHAPTER-I

# INTRODUCTION

## 1.1 MOTIVATION :

Fluid-dynamics theory, for reasons of history and fashion, has paid little attention to the phenomena which occur in industrial equipment such as heat exchangers, cooling towers etc. Even now, when the digital computers have removed the obstacles of numerical computation, the prized achievements of applied mathematicians concern more often the supersonic flow of air about a missile, or the development of an eddy behind a cylinder, than any phenomenon of interest to a process engineer.

As a consequence, the designer of process equipment must usually base predictions of its performance on assumptions about the flow patterns, departures from these assumptions are then allowed for by empirically-derived correction formulae. Thus a single pass shell and tube heat exchanger may be designed by reference to the formula for the performance of an ideal counter flow heat exchanger, modified by some performance degradation factor which takes account of departures from ideal flow pattern.

Unfortunately, although this practice can serve adequately for interpolation between equipment items of common type with only slight variations of geometry, it fails completely where the benefit of new geometrical configurations is to be explored; optimum configurations must, therefore, be determined experimentally as a rule. None the less doing an experiment using a model is not an easy task. Besides, it is a time consuming and costly affair compared with its equivalent computational work.

The present work is an attempt to introduce a new fashion in flow modeling of process equipment, by applying to a shell and tube heat exchanger a numerical procedure for calculating the fluid-flow field.

The shell side flow is considered as a two dimensional flow of liquid through a porous medium which consists of tube bundles. The flow-field on shell side is calculated using finite-element method. The tube side flow is assumed to be one-dimensional. Both the liquids on shell and tube side remain in liquid state throughout the space inside the heat exchanger. The whole analysis is done for steady-state operation of the heat exchanger.

## 1.2 ORGANISATION OF THESIS :

The organisation of thesis is a simple one. The thesis is divided into four chapters excluding the present one.

Chapter two is a literature survey related to the present problem and its relation to the present work undertaken. The objectives of the present work are also listed in this chapter.

Chapter three describes the modeling techniques used for finding out the velocity fields on shell side of the heat exchanger. The governing differential equations and the formulation are discussed here.

Chapter four describes the solution procedure and the programme for the calculation of velocity field inside the heat exchanger. The computational method employed for the solution of algebraic equations is also given in this chapter.

Chapter five gives the discussion of results and the conclusions. The limitations of the present work and the scope for future work are also discussed in this chapter. This chapter is followed by a list of references.

# CHAPTER- II

# LITERATURE SURVEY

## 2.1 REVIEW OF THE EXISTING MODELS :

A few simplified models are available for the steady-state analysis of shell and tube heat exchangers. Almost all of them are developed for the analysis of steam generators.

The fundamental conservation principles are applied in all the models developed so far. The differences in the various formulations available lie in the way the conservation equations are written, the assumptions and the approximations in the equations. The models available are either one-dimensional or three-dimensional and use Finite-Difference technique in most of the cases, for the solution of the problem.

The idea of using distributed resistances to simulate the presence of heat transfer tubes and baffle plates on the shell side of a heat exchanger was first introduced by Patankar and Spalding [1974]. They had assumed that the space inside a heat exchanger was uniformly filled with fluid, throughout which, however a resistance to fluid motion was distributed on a fine scale. They did

not calculate tube-side flow distribution. The model was developed using continuum approach by finite-difference scheme. Diffusion and shear-forces were not taken into account while simulating the model. Also the authors assumed constant density, throughout the calculation domain.

More recently AbuRomia et al. [1976] applied the distributed resistance concept to obtain the flow field between the typical tube support spans of the Clinch River Breeder Reactor plant (CRBRP) Intermediate Heat Exchangers.

Patankar et. al. [1980] developed a computer code which was a three-dimensional finite-difference analysis for predicting the local thermal/hydraulics of nuclear once-through generators. The tube bundle and tube-support plates were modeled as a porous media with distributed resistance to flow. They used quasi-continuum approach and solved a steady state, fully elliptic set of governing equations for the simulation.

A complicated analysis of Shell and Tube Heat Exchangers using finite-difference method was given by Sha et. al.[1982]. They also used continuum approach to solve Navier-Stoke's equations which were modified to represent the phenomenon in a heat exchanger, in cylindrical

co-ordinates. They considered volume porosity as well as surface permeability to model the flow. Since, in general, the tube bundle porosity and permeability are anisotropic, they used a combination of porosity, permeability and distributed resistance for the analysis of flow-field. Surface permeability was defined as the fraction of open projected flow area in the direction of flow component in the control volume. They had also developed a one-equation turbulence model for a tube bundle based on transport equation for the turbulent kinetic energy. The model took into account the effect of diffusion and shear forces.

One dimensional analysis for steam generator transients was given by Bhatnagar [1983] using finite difference technique.

## 2.2 PRESENT WORK :

Present work is an attempt to reduce the complications of three-dimensional analysis and yet simulate the steady state flow-field inside a single phase shell and tube heat exchanger. A combination of volume porosity and distributed resistance is used in the simulation process. The effect of diffusion is also considered in the conservation equations. A continuum approach is followed throughout the calculation domain.

The analysis is done using two-dimensional conservation equations modified to represent the process in a shell and tube heat exchanger. The momentum and continuity equations are solved simultaneously using finite-element technique. The whole domain is divided into eight noded isoparametric elements. The Galerkin Weighted Residual method is used for obtaining the flow field and a three Gauss-point Numerical Integration is used for evaluating various integrals. Pressure formulation is used to solve the equations. The density of shell-side fluid was taken to be uniform throughout the domain, though the inclusion of their variations in the calculation procedure will present no difficulty.

The objectives of the present work are :

1. To simulate the flow field inside single phase flow shell and tube heat exchangers.
2. to explore the possibility of using the above mentioned approach for effective modeling of heat exchangers.

# CHAPTER-III

## FINITE ELEMENT FORMULATION OF FLOW EQUATIONS

### 3.1 PROBLEM DEFINITION :

Figure 3.1 shows a shell and tube heat exchanger with both the shell and tube sides arranged for a single-pass flow.

Shell-side fluid enters the heat exchanger through inlet (N-1) and comes out of the heat exchanger through outlet (N-2). The orientation of heat exchanger with respect to x,y and z axes is also shown in the same Figure. From the geometry of the shell and tube heat exchanger shown, one can see that the major directions along which the fluid flows occur are X and Y directions. The flow in Z- direction is negligible.

Further, the tube side fluid enters the heat exchanger at a uniform temperature in the X-direction. The shell-side fluid enters perpendicularly, also at a uniform temperature in the Y-direction. Hence the first row of tubes, which is at uniform temperature, will come in contact with shell-side fluid which is also at uniform temperature. Thus after passing the first row, the shell-

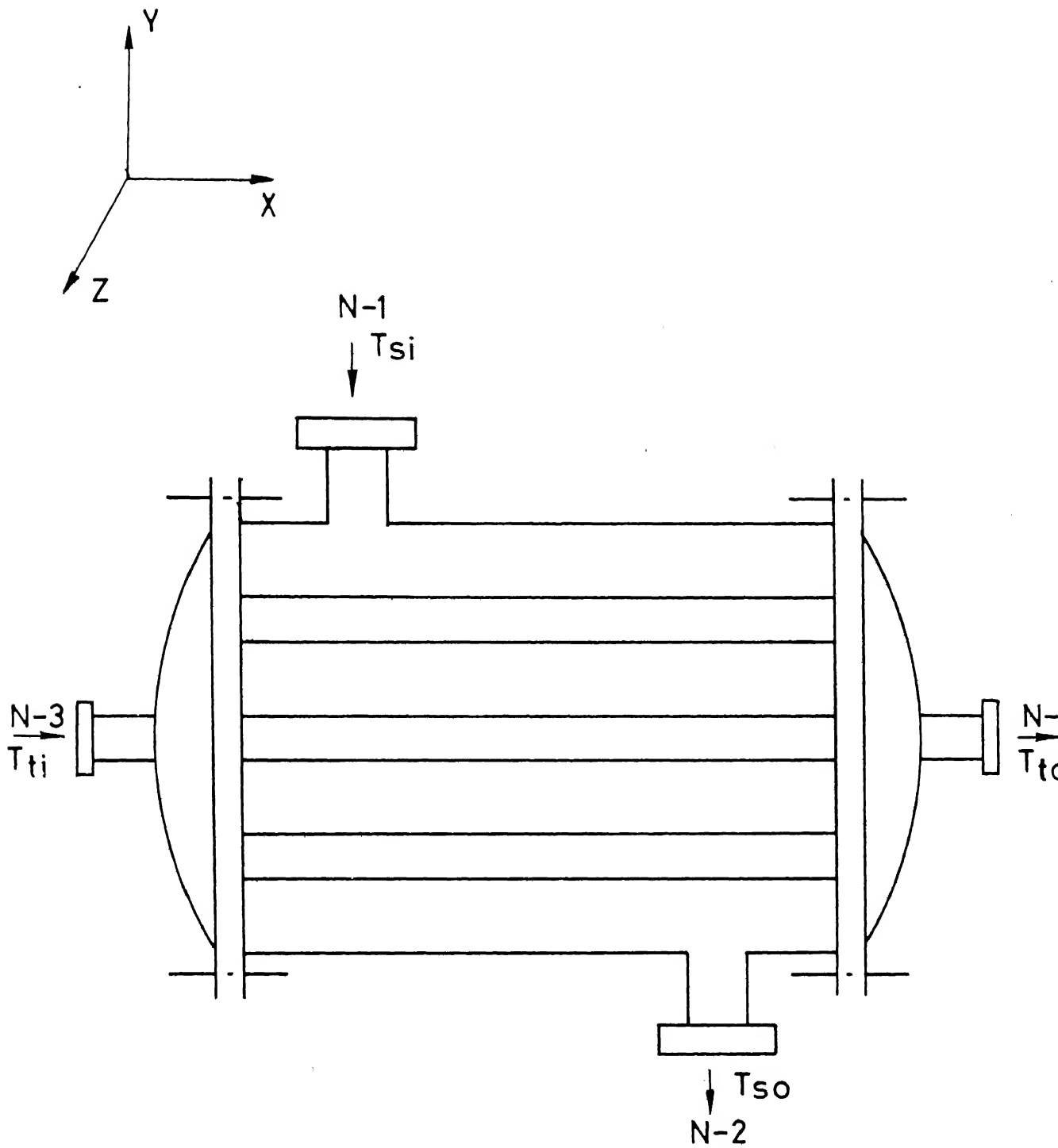


Fig. 3.1 Shell and Tube Heat Exchanger

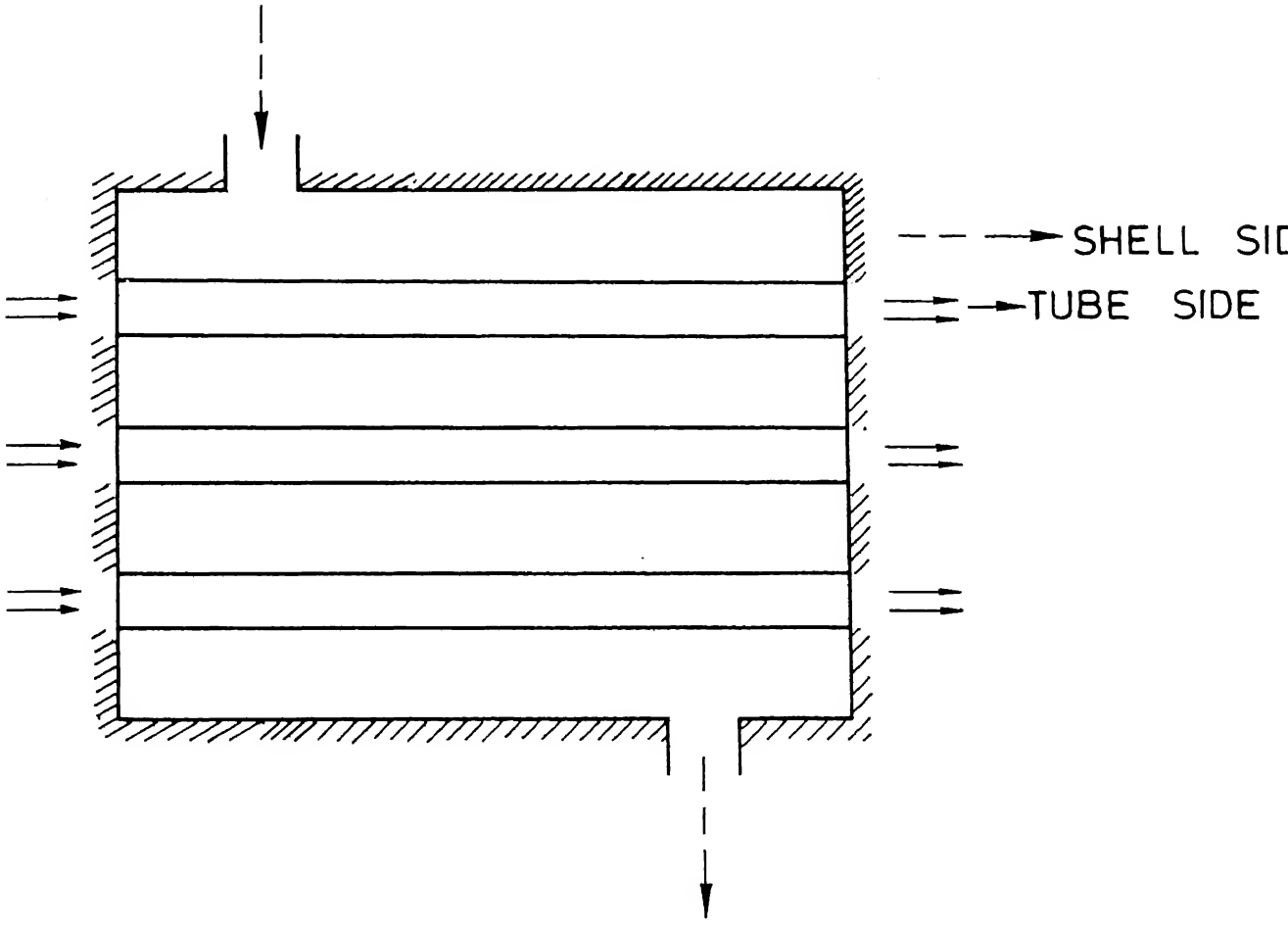


Figure 3.2 Two Dimensional Calculation Domain

side fluid will be more or less at a uniform temperature. Hence it can be concluded without comitting a serious error that the shell-side fluid has temperature gradients only in the X-and Y-directions. For the same reasons, the tube-side fluid will also have temperature gradients in X and Y directions only. Hence the possibility of flow due to temperature gradient or natural convection currents is reduced in the Z-direction.

For the reasons mentioned above, one can reduce the problem to two dimensions though with introduction of a slight error. For the tube side fluid the flow can be safely considered as unidirectional since the diameter of tube is generally small to allow the approximation.

## 3.2 GOVERNING DIFFERENTIAL EQUATIONS :

Figure 3.2 shows the diameteral section of a shell and tube heat exchanger in the X-Y plane. For simplicity, the inlet and outlet nozzle lengths are neglected. momentum and the continuity equations which govern the steady state flow of the shell-side fluid are given below.

X-direction momentum equation -

$$u \frac{\partial u}{\partial x} + v \frac{\partial u}{\partial y} = \frac{f_x L}{\rho_s u_o^2} - \frac{\partial p}{\partial x} + \frac{\nu_s}{u_o L} \left( \frac{\partial^2 u}{\partial x^2} + \frac{\partial^2 u}{\partial y^2} \right) \quad .... (3.1)$$

Y-direction momentum equation -

$$u \frac{\partial v}{\partial x} + v \frac{\partial v}{\partial y} = \frac{f_y L}{\rho_s u_o^2} - \frac{\partial p}{\partial y} + \frac{\nu_s}{u_o L} \left( \frac{\partial^2 v}{\partial x^2} + \frac{\partial^2 v}{\partial y^2} \right) \quad .....(3.2)$$

continuity equation -

$$\frac{\partial u}{\partial x} + \frac{\partial v}{\partial y} = 0 \quad ..... (3.3)$$

Where each term in the above equations is non-dimensionalized using the following parameters

$$x = \frac{x^*}{L}, y = \frac{y^*}{L}, \quad u = \frac{u^*}{u_o}, \quad v = \frac{v^*}{u_o}$$

and $$p = \frac{p^*}{\rho_s u_o^2} \quad ..... (3.4)$$

The left hand side of the momentum equations represents the convection terms and the second order terms on the right hand side represent the diffusion terms. The body forces appearing on the right hand side include (1) the weight of the fluid and (2) the distributed resistance in the x or y direction due to the presence of the tubes. It may be noted that the density appearing in the above equations is a fraction of the element volume filled by the shell-side fluid. This takes into account volume

porosity of the element. The porosity will, thus, have a value in the range of 0 to 1. Throughout the analysis, the porosity is assumed to be a continuous parameter just as any other variable. In essence, the concept of porosity essentially smears the effect of flow obstruction over the complete element volume. The location of the obstruction within the control volume is not specified. The porosity, as used in the current analysis, is then a scalar quantity and does not vary with spatial coordinates.

## 3.3 DISTRIBUTED RESISTANCE :

The following discussion presents a general description of the models used for the calculation of distributed resistances (Patankar, et.al., 1980).

As mentioned earlier, the effect of obstruction due to the presence of tubes is modeled using the concept of distributed resistance which represents the force of obstruction per unit volume of the shell side fluid. These resistances are present in the X and Y-directions only.

### 3.3.1 X-Direction Resistance ($R_x$) :

This resistance accounts for the pressure drop due to flow over the tube in the axial direction. This is calculated from (Patankar, 1980).

$$R_x = -2f \frac{\rho_s u . q}{d_h} \qquad \text{.....(3.5)}$$

3.2.2 Y-Direction Resistance ($R_y$):

This resistance accounts for the pressure drop due to flow perpendicular to the length of tube i.e. This is a cross-flow resistance and is calculated using (Patankar, 1980).

$$R_y = -4 f_r \frac{G . q}{t_p} \qquad \text{.... (3.6)}$$

where $$G = \frac{\rho_s v . t_p}{(t_p - d)} \qquad \text{.... (3.7)}$$

The resistances defined above are included in the body force terms in the conservation equations along with the weight of the fluid which may act in any direction depending upon the orientation of the heat exchanger.

## 3.4 FORMULATION FOR THE SHELL SIDE :

The governing differential equations (3.1), (3.2) and (3.3) are solved simultaneously to obtain velocities inside the heat exchanger.

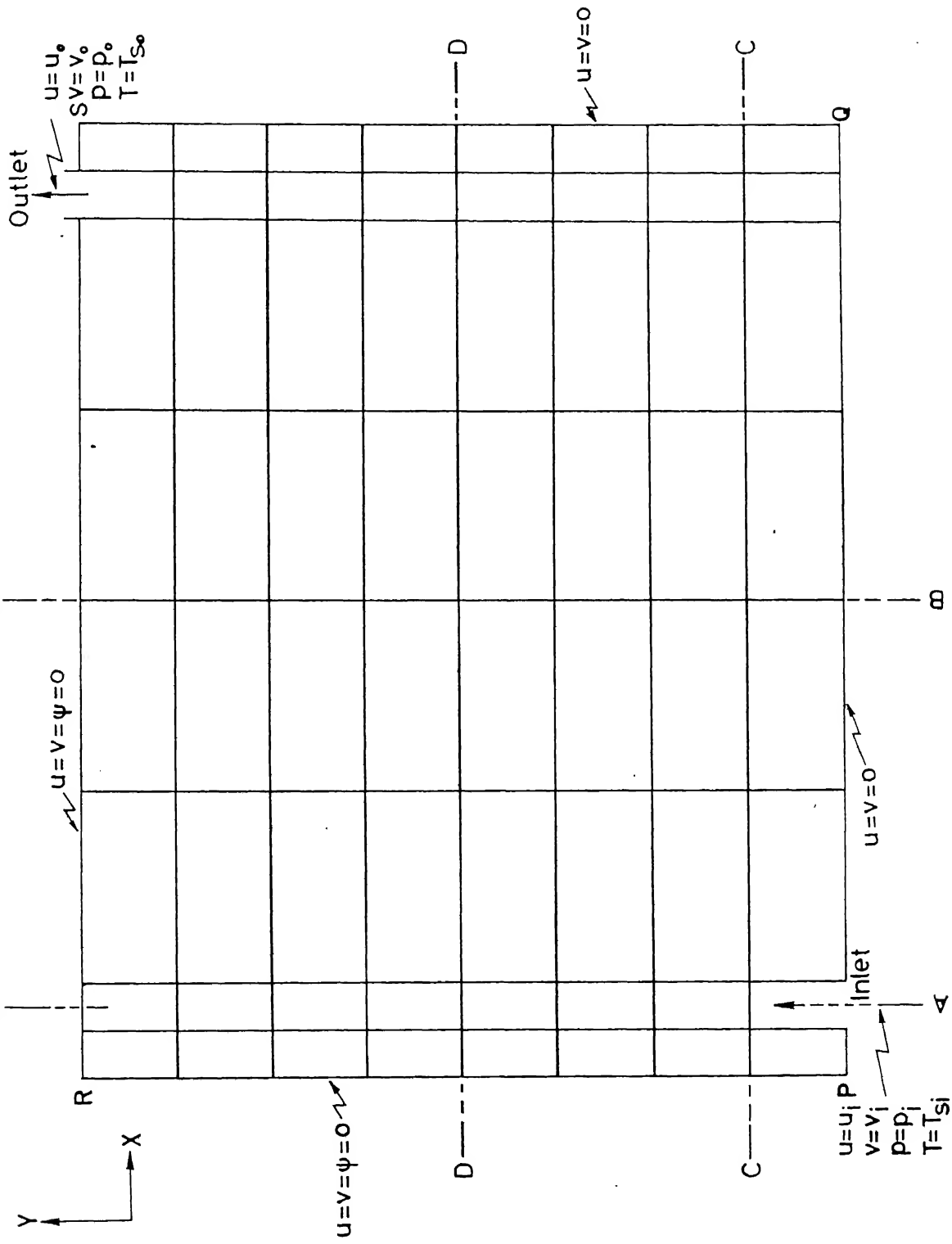


Fig. 3.3 Finite Element Mesh

Figure 3.3 shows the calculation domain along with the boundary conditions for the shell side. No slip boundaries are considered so that along the boundary, velocity in any direction is zero. Further, the fluid is assumed to enter the heat exchanger at a uniform velocity. The calculation domain is divided into a number of elements as shown. Hence u and v-velocities are known at any point on the boundary. Further the pressure at the inlet is known.

The variables u, v and p are represented for a particular element using a polynomial which is function of the local coordinates for that element. These are nothing but the shape functions which are evaluated at Gauss points. Following an accepted practice of depicting the variation in pressure by shape functions of one order lower than those for defining the velocity distribution.

$$u = \sum_{i=1}^{n} N_i \, u_i \qquad \ldots (3.8a)$$

$$v = \sum_{i=1}^{n} N_i \, v_i \qquad \ldots . (3.8b)$$

$$p = \sum_{i=1}^{m} M_i \, p_i \qquad \ldots . (3.8c)$$

where n = 8 and m =4

The requirement is fulfilled by utilising a rectangular isoparametric element with eight nodes where all the eight nodes are associated with velocity and only corner nodes are associated with pressure . Spatial co-ordinates within the element are defined in terms of co-ordinates of the eight nodes. The element is shown in Figure 3.4.

3.4.1 Shape Functions :

As stated earlier, shape functions are weighting functions, used to depict the variation of a variable in a particular domain. Once the calculation domain is divided into a number of elements, each element has certain number of nodes. The values of a particular variable on these nodes are used to define the variation of that variable inside the element (see equation (3.8)).

Referring to Figure 3.4, the element shown has eight nodes, four corner nodes and four mid-side nodes. It may be noted that each side of the element has three nodes. Hence this element can accomodate a parabolic variation in the variable along any side of and across the element and is called a parabolic element.

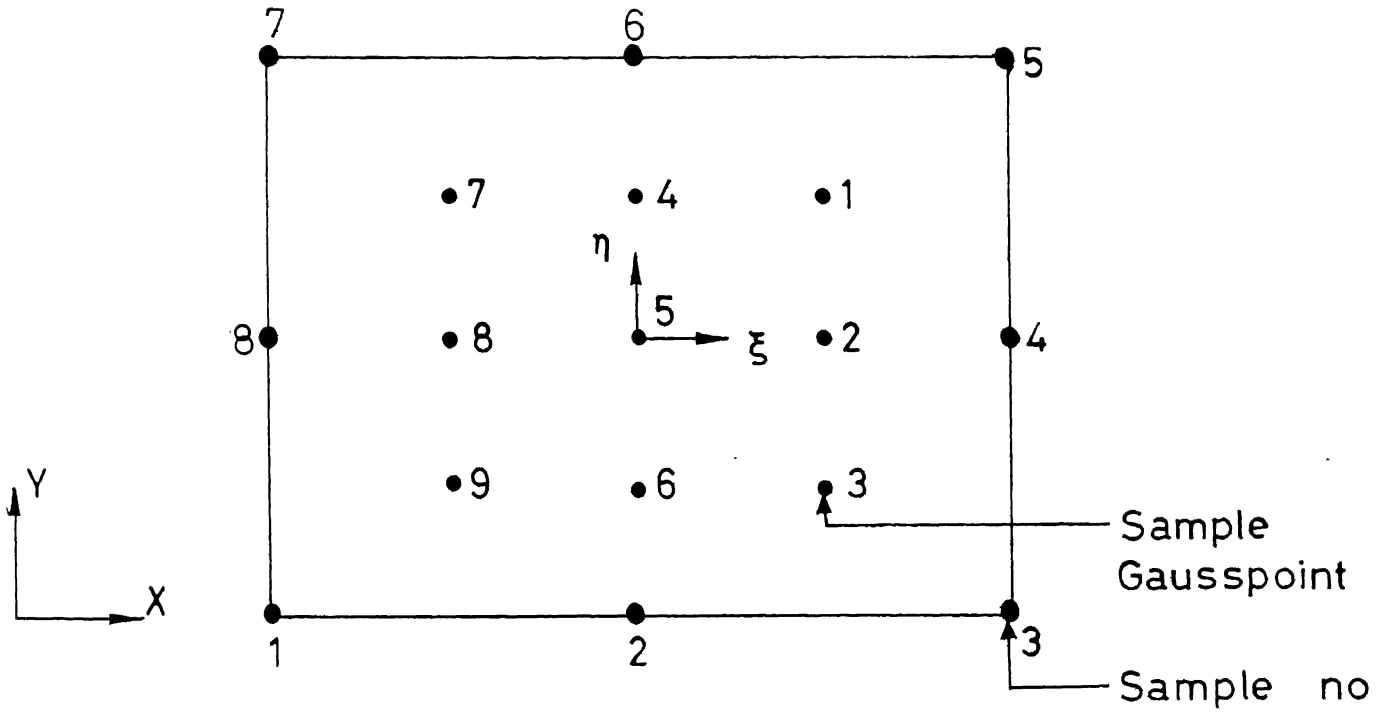


ξ - η - Local Co-ordinate System
X-Y Global Co-ordinate System

Figure 3.4 Eight Noded Rectangular Element with Nine Gauss Points

Shape function is a polynomial defined using a local co-ordinate system for the element. This is a normalised co-ordinate system, defined for each element in the domain. The shape functions used here are

i) Corner nodes

$$N_i = \frac{1}{4}(1+\varepsilon_i\varepsilon)(1+\eta_i\eta)(\varepsilon_i\varepsilon + \eta_i\eta - 1) \quad \ldots\ldots (3.9a)$$

ii) Mid-side nodes

$$N_i = \frac{1}{2}(1+\eta_i\eta)(1-\varepsilon^2),\ \varepsilon_i = 0 \quad \ldots\ldots (3.9b)$$

$$N_i = \frac{1}{2}(1+\varepsilon_i\varepsilon)(1-\eta^2),\ \eta_i = 0 \quad \ldots\ldots (3.9c)$$

Where $\varepsilon_i$ and $\eta_i$ are local co-ordinates of $i^{th}$ node.

To relate local co-ordinate system with global co-ordinate system, again the same shape functions are used i.e. the variation of global co-ordinates inside an element is depicted by the same shape functions. Hence

$$x = \Sigma N_i x_i \quad \ldots\ldots (3.10a)$$

$$y = \Sigma N_i y_i \quad \ldots\ldots (3.10b)$$

Where x and y refer to global co-ordinates of a point inside an element and $x_i$ and $y_i$ are global co-ordinates of $i^{th}$ node. It may be noted that the value of a shape function evaluated at a nodal point will be unity, since at a nodal point the value of the variable is already specified. The element used here is isoparametric because same shape functions are used to define the variation in global co-ordinates and the variable variation within an element. Once the shape functions are evaluated at a point inside an element, the values of any variable as well as global co-ordinates at that point can be determined. In present case (see Figure 3.4), there are nine Gauss points inside an element and each Gauss point will have eight shape functions. Hence there will be seventy two shape function values for each element.

3.4.2 Variable Derivative :

If a derivative of particular variable inside an element is required, it can readily be calculated using shape functions. Thus

$$\frac{\partial u}{\partial x} = \sum_{i=1}^{8} \left( \frac{\partial N_i}{\partial x} \right) u_i \qquad \ldots\ldots (3.11)$$

Since nodal values of a variable are constant.

The derivatives of shape functions with respect to global co-ordinates (see equation (3.11)) can be calculated using chain rule of partial differentiation.

$$\frac{\partial N_i}{\partial \varepsilon} = \frac{\partial N_i}{\partial x}\frac{\partial x}{\partial \varepsilon} + \frac{\partial N_i}{\partial y}\frac{\partial y}{\partial \varepsilon} \quad \ldots\ (3.12a)$$

$$\frac{\partial N_i}{\partial \eta} = \frac{\partial N_i}{\partial x}\frac{\partial x}{\partial \eta} + \frac{\partial N_i}{\partial y}\frac{\partial y}{\partial \eta} \quad \ldots\ (3.12b)$$

which may be written as

$$\begin{bmatrix} \partial N_i/\partial \varepsilon \\ \partial N_i/\partial \eta \end{bmatrix} = \begin{bmatrix} \partial x/\partial \varepsilon & \partial y/\partial \varepsilon \\ \partial x/\partial \eta & \partial y/\partial \eta \end{bmatrix} \begin{bmatrix} \partial N_i/\partial x \\ \partial N_i/\partial y \end{bmatrix}$$

$$\begin{bmatrix} \partial N_i/\partial \varepsilon \\ \partial N_i/\partial \eta \end{bmatrix} = J \begin{bmatrix} \partial N_i/\partial x \\ \partial N_i/\partial \eta \end{bmatrix} \quad \ldots\ (3.13)$$

Inverting J to find the global variation in shape functions,

$$\begin{bmatrix} \partial N_i/\partial x \\ \partial N_i/\partial y \end{bmatrix} = J^{-1} \begin{bmatrix} \partial N_i/\partial \varepsilon \\ \partial N_i/\partial \eta \end{bmatrix} \quad \ldots\ (3.14)$$

Where J is Jacobian and can be evaluated explicitly since the local variation in x and y can be defined.

$$J = \begin{bmatrix} \sum_{i=1}^{8} \left(\frac{\partial N_i}{\partial \varepsilon}\right) x_i & \sum_{i=1}^{8} \left(\frac{\partial N_i}{\partial \varepsilon}\right) y_i \\ \sum_{i=1}^{8} \left(\frac{\partial N_i}{\partial \eta}\right) x_i & \sum_{i=1}^{8} \left(\frac{\partial N_i}{\partial \eta}\right) y_i \end{bmatrix} \quad \ldots\ldots (3.15)$$

The inverse of Jacobian can be found out using standard matrix inversion technique.

$$J^{-1} = \begin{bmatrix} \frac{\partial \varepsilon}{\partial x} & \frac{\partial \eta}{\partial x} \\ \frac{\partial \varepsilon}{\partial y} & \frac{\partial \eta}{\partial y} \end{bmatrix} = \frac{1}{\det J} \begin{bmatrix} \frac{\partial y}{\partial \eta} & -\frac{\partial y}{\partial \varepsilon} \\ -\frac{\partial x}{\partial \eta} & \frac{\partial x}{\partial \varepsilon} \end{bmatrix} \quad \ldots\ldots (3.16)$$

$$\det J = \frac{\partial x}{\partial \varepsilon} \cdot \frac{\partial y}{\partial \eta} - \frac{\partial x}{\partial \eta} \cdot \frac{\partial y}{\partial \varepsilon} \quad \ldots\ldots (3.17)$$

It may be noted that

$$dx\, dy = (\det J)\, d\varepsilon\, d\eta \quad \ldots\ldots (3.18)$$

3.4.3 Algebraic Equations.

Employing the Galerkin's weighted residual approach, in which same approximating functions are used for the weighting and trial functions and using equation (3.8), equation (3.1) becomes

$$\sum_{1}^{ne} \int_{A^e} N_i \Big[ \sum_{1}^{n} N_k u_k \sum_{1}^{n} \frac{\partial N_j}{\partial x} u_j + \sum_{1}^{n} N_k V_k \sum_{1}^{n} \frac{\partial N_j}{\partial y} u_j$$

$$+ \sum_{1}^{m} \frac{\partial M_l}{\partial x} p_l - \frac{f_x L}{\rho_s u_o^2} - \frac{1}{Re_s}\Big( \sum_{1}^{n} \frac{\partial^2 N_j}{\partial x^2} u_j + \sum_{1}^{n} \frac{\partial^2 N_j}{\partial y^2} u_j \Big) \Big] dA^e = 0 \quad \ldots. (3.19)$$

Where the outer summation refers to each element in the domain and the inner summations to the appropriate number of nodes in an element. In the present case, n=8 and m=4.

Invoking Green's theorem, the order of the second order terms can be reduced leading to the expression.

$$\int_{A^e} N_i \Big[ \sum_{1}^{n} \frac{\partial^2 N_j}{\partial x^2} u_j + \sum_{1}^{n} \frac{\partial^2 N_j}{\partial y^2} u_j \Big] dA^e$$

$$= \int_{C^e} N_i \sum_{1}^{n} \frac{\partial N_j}{\partial n} u_j \, ds - \int \Big[ \frac{\partial N_i}{\partial x} \sum_{1}^{n} \frac{\partial N_j}{\partial x} u_j + \frac{\partial N_i}{\partial y} \sum_{1}^{n} \frac{\partial N_j}{\partial y} u_j \Big] dA^e$$

$\ldots.$ (3.20)

Where $C^e$ denotes the element surface. When these are summed over the adjacent element elements, the final contribution of the mass flux becomes zero unless a boundary acts as a limit to the domain.

Substituting equation (3.20) into equation (3.19)

$$\sum_{1}^{ne} \Big[\int \Big(N_i N_k u_k \frac{\partial N_j}{\partial x} u_j + N_i N_k v_k \frac{\partial N_j}{\partial y} u_j + N_i \frac{\partial M_l}{\partial x} p_l - N_i \frac{f_x L}{\rho_s u_o^2} + \frac{1}{Re_s}\Big( \frac{\partial N_i}{\partial x}\frac{\partial N_j}{\partial x} u_j + \frac{\partial N_i}{\partial y}\frac{\partial N_j}{\partial y} u_j\Big)\Big) dA^e\Big]$$

$$- \int_{C^e} \frac{1}{Re_s} N_i \frac{\partial N_j}{\partial n} u_j \, dC^e = 0 \qquad \ldots\ (3.21)$$

where $l = 1 \ldots 4$

$j = 1 \ldots 8$

$k = 1 \ldots 8$

$i = 1 \ldots$ No. of points.

The corresponding momentum equation in the Y-direction is obtained by simply interchanging x,y and u,v in equation (3.21). Substituting equation (3.8) into equation (3.3) yields, the continuity equation as

$$\sum_{1}^{ne} \int M_i \left( \frac{\partial N_j}{\partial x} u_j + \frac{\partial N_j}{\partial y} v_j \right) dA^e = 0 \qquad \ldots\ (3.22)$$

Where the weighting function is now taken as $M_i$ associated with four nodes only as far as the pressure is concerned.

The above equations are written for each element of the calculation domain and are solved simultaneously to obtain the velocities in the domain.

The assembled matrix equations take the form

$$A\lambda = F+B \qquad \ldots\ (3.23)$$

where for the node i, the chosen form for $\lambda$ is

$$\lambda_i = \begin{bmatrix} u_i \\ p_i \\ v_i \end{bmatrix}$$

Each coefficient in the matrix A has the form

$$a_{ij} = \sum_{1}^{ne} \int_{A^e} \begin{bmatrix} C_{11} & C_{12} & C_{13} \\ C_{21} & C_{22} & C_{23} \\ C_{31} & C_{32} & C_{33} \end{bmatrix} dA^e$$

$$- \int_{C^e} \begin{bmatrix} \frac{1}{Re_s} N_i \frac{\partial N_j}{\partial n} & 0 & 0 \\ 0 & 0 & 0 \\ 0 & 0 & \frac{1}{Re_s} N_i \frac{\partial N_j}{\partial n} \end{bmatrix} dC^e$$

.... (3.24)

where

$$C_{11} = N_i N_k \bar{u}_k \frac{\partial N_j}{\partial x} + N_i N_k \bar{v}_k \frac{\partial N_j}{\partial y}$$

$$+ \frac{1}{Re_s} \left( \frac{\partial N_i}{\partial x} \frac{\partial N_j}{\partial x} + \frac{\partial N_i}{\partial y} \frac{\partial N_j}{\partial y} \right)$$

$$C_{12} = N_i \frac{\partial M_l}{\partial x}, \qquad C_{13} = 0, \qquad C_{21} = M_i \frac{\partial N_j}{\partial x}$$

$$C_{22} = 0, \qquad C_{23} = M_i \frac{\partial N_j}{\partial y}, \qquad C_{31} = 0$$

$$C_{32} = N_i \frac{\partial M_j}{\partial y} \quad \text{and} \quad C_{33} = C_{11} \qquad \text{.... (3.25)}$$

In the expression for $C_{11}$, $\bar{u}_k$ and $\bar{v}_k$ denote the velocities obtained from the previous iteration or the guessed velocities, since the equations to be solved are non-linear. In the present case, since all the boundary conditions are of essential type, the surface integral in equation (3.24) is not required and can be equated to zero.

The first matrix on right hand side corresponds to the body forces and is written as

$$f_i = \sum_{1}^{ne} \int_{A^e} \begin{bmatrix} f_1 \\ f_2 \\ f_3 \end{bmatrix} dA^e \qquad \ldots\ldots (3.26)$$

where $f_1 = N_i \dfrac{f_x L}{\rho_s u_o^2}$, $f_2 = 0$, $f_3 = N_i \dfrac{f_y L}{\rho_s u_o^2}$ $\ldots\ldots (3.27)$

The second matrix on the right hand side consists of the velocity gradient terms on the boundary. In the present case, complete boundary is known and therefore this matrix is not required. It can be seen by examining terms such as $N_i N_k \bar{u}_k \dfrac{\partial N_j}{\partial x}$ that the interchange of i and j results in a non-symmetric matrix.

3.4.4 Elemental Matrix :

Referring to Figure 3.4, the element shown has eight nodes and it is already stated that corner nodes are associated with pressures and velocities where as midside nodes are associated with velocities only. Hence each corner node has three degrees of freedom (u-velocity, v-velocity and pressure) and a mid-side node has only two degrees of freedom (u-velocity and v-velocity). Thus each element will have 20 degrees of freedom. The momentum and the continuity equations when written for an element will give rise to a 20x20 matrix on left hand side as shown below.

$$
\begin{array}{ll}
\text{1st Row} & \left[\begin{array}{cccccc}
a_{1,1} & a_{1,2} & a_{1,3} & a_{1,4} & a_{1,5} \cdots & a_{1,20} \\
a_{2,1} & a_{2,2} & a_{2,3} & a_{2,4} & a_{2,5} \cdots & a_{2,20} \\
a_{3,1} & a_{3,2} & a_{3,3} & a_{3,4} & a_{3,5} \cdots & a_{3,20} \\
\vdots & & & & & \\
a_{20,1} & a_{20,2} & a_{20,3} & a_{20,4} & a_{20,5} \cdots & a_{20,20}
\end{array}\right] \\
\text{2nd Row} & \\
\text{3rd Row} &
\end{array}
\qquad (20x20)
$$

Where the coefficients are already defined in equation (3.24).

In above matrix 1st, 2nd and 3rd rows are obtained by writing X-direction momentum, continjity and Y-direction momentum equations respectively. The variable matrix for each element will be a column matrix of (20x1) as shown below.

$$\begin{bmatrix} u_1 \\ p_1 \\ v_1 \\ u_2 \\ v_2 \\ u_3 \\ p_3 \\ v_3 \\ \cdot \\ \cdot \\ \cdot \\ u_8 \\ v_8 \end{bmatrix}_{(20x1)}$$

3.4.5 Global Matrix :

The elemental matrix defined in section 3.4.4 is obtained for each element and all such matrices are assembled to obtain the global matrix. It may be noted that

while assembling the elemental matrices, some nodes will be common for more than one element. In such a case, the contributions from all the elements for that particular node are added and global matrix element for that node is calculated. The global matrix will be a square NxN matrix of order N, where N is the total number of degrees of freedom for all the nodes in the calculation domain.

3.4.6 Boundary Conditions :

In the present case, velocities are known along the entire boundary and pressure is known at the inlet. To illustrate the incorporation of boundary conditions in global matrix, a (4x4) matrix is considered below.

$$\begin{bmatrix} a_{11} & a_{12} & a_{13} & a_{14} \\ a_{21} & a_{22} & a_{23} & a_{24} \\ a_{31} & a_{32} & a_{33} & a_{34} \\ a_{41} & a_{42} & a_{43} & a_{44} \end{bmatrix} \begin{bmatrix} u_1 \\ u_2 \\ u_3 \\ u_4 \end{bmatrix} = \begin{bmatrix} F_1 \\ F_2 \\ F_3 \\ F_4 \end{bmatrix} \quad \ldots\ldots (3.28)$$

Assume that $u_2$ is known and is equal to $u'$, then the incorporation of this boundary condition in global matrix yields.

$$\begin{bmatrix} a_{11} & 0 & a_{13} & a_{14} \\ 0 & 1 & 0 & 0 \\ a_{31} & 0 & a_{33} & a_{34} \\ a_{41} & 0 & a_{43} & a_{44} \end{bmatrix} \begin{bmatrix} u_1 \\ u_2 \\ u_3 \\ u_4 \end{bmatrix} = \begin{bmatrix} F_1 - a_{12}\, u' \\ u' \\ F_3 - a_{13}\, u' \\ F_4 - a_{14}\, u' \end{bmatrix}$$

which can be reduced to

$$\begin{bmatrix} a_{11} & a_{13} & a_{14} \\ a_{31} & a_{33} & a_{34} \\ a_{41} & a_{43} & a_{44} \end{bmatrix} \begin{bmatrix} u_1 \\ u_3 \\ u_4 \end{bmatrix} = \begin{bmatrix} F_1 - a_{12}\, u' \\ F_3 - a_{13}\, u' \\ F_4 - a_{14}\, u' \end{bmatrix} \quad \ldots\ (3.29)$$

For a zero value at the boundary, equation (3.29) can be written as

$$\begin{bmatrix} a_{11} & a_{13} & a_{14} \\ a_{31} & a_{33} & a_{34} \\ a_{41} & a_{43} & a_{44} \end{bmatrix} \begin{bmatrix} u_1 \\ u_3 \\ u_4 \end{bmatrix} = \begin{bmatrix} F_1 \\ F_3 \\ F_4 \end{bmatrix} \quad \ldots\ (3.30)$$

### 3.4.7 Numerical Integration

For evaluating the coefficients $a_{ij}$ in equation (3.24), the numerical integration is carried out using a 3x3 Gauss point scheme. The sample gauss points are shown in Figure 3.4. The method used to carry out the numerical integration is as follows.

For each element the integrand can be written as

$$I = \int_{-1}^{+1} \int_{-1}^{+1} F(\varepsilon, \eta)\, d\varepsilon \; d\eta \qquad \ldots\ (3.31)$$

where $\varepsilon$ and $\eta$ are local normalised co-ordinates. The integrand can be written as

$$I = \int_{-1}^{+1} \left( \int_{-1}^{+1} F(\varepsilon, \eta)\, d\varepsilon \right) d\eta \qquad \ldots\ (3.32)$$

First carrying out the integration within the parentheses

$$I = \int_{-1}^{+1} \left[ \sum_{i=1}^{m_1} a_i\, F(\varepsilon_i, \eta) \right] d\eta \qquad \ldots\ (3.33)$$

The integrand is now a function of $\eta$ only and hence

$$I = \sum_{j=1}^{m_2} a_j \sum_{i=1}^{m_1} a_i\, F(\varepsilon_i, \eta_i) \qquad \ldots\ (3.34)$$

or

$$I = \sum_{j=1}^{j=m_2} \sum_{i=1}^{m_1} a_j\, a_i\, F(\varepsilon_i, \eta_i) \qquad \ldots\ (3.34)$$

Here a 3x3 Gaussian integration is adopted hence $m_1 = m_2 = 3$, where $a_i$ and $a_j$ are the weighting factors for $i^{th}$ and $j^{th}$ Gauss points respectively.

## 3.5 ITERATIVE PROCEDURE :

The set of non-linear simultaneous equations given by equation (3.23) is solved by an iterative process in which a simple convergence sequence and a method of variable updating is employed. The procedure can be summarised as :

i) Assume initial values of the variable u, p and v

ii) Solve the matrix equations (3.23) to obtain new values of u, p and v at node points.

iii) Evaluate the differences $(u-u')/u$, $(v-v')/v$ and $(p-p)/p'$. If these are within the specified tolerance at all points then the calculation is complete.

iv) If the differences calculated above are not within the required tolerance then using suitable under-relaxation determine the new values of u, p and v.

The steps (i) to (iv) are repeated until convergence is obtained.

# CHAPTER- IV

## PROGRAMS AND PROCEDURES

### 4.1 SUBROUTINES :

The program is made up of following subroutines.

1. DIMENS.

A number of vectors and arrays are utilized during house-keeping process involved in the formulation of the matrix to be solved. The dimension required for each of these vectors or arrays is set in subroutine DIMENS. This permits a form of dynamic dimensioning to be used. The program can, therefore, be increased or decreased in size to suit a particular grid size.

2. DINPUT.

The data required are read in subroutine DINPUT. This includes physical properties of the shell-side fluid and boundary conditions. As the data are given to two other subroutines DIAGN1 and DIAGN2, they are called in to check that the data which are given comply with the required checks.

3. DIAGN1.

This subroutine checks the overall control parameter which governs the number of nodes, number of elements and the boundary conditions for the particular problem under investigation.

4. DIAGN2.

Various checks are incorporated to ensure that the geometric data obey simple criteria. If any check fails, the data which are not read to that point will be read and printed.

5. DRIVES.

A subroutine in which the constants necessary for numerical integration of the relevant equations are defined. Subroutines SHAPE8, SHAPE4 and DJACOB are called from DRIVES.

6. SHAPE8.

The subroutine SHAPE8 calculates the shape functions, required for defining the variation of the independent variable over an element which contains eight nodes on the element boundary.

7. SHAPE4.

This subroutine calculates the shape functions for a four noded element. Two shape function subroutines are used in the program since the pressure and velocity in the Navier-Stokes equations here are associated with four and eight nodes of an element respectively.

8. DJACOB.

In this subroutine, the first order differentials of the shape functions, with respect to the chosen co-ordinate

system, are calculated. These are required when terms such as $\frac{\partial u}{\partial x}$ , $\frac{\partial u}{\partial y}$ are to be calculated. For instance, having defined.

$$u = \begin{bmatrix} N_1, N_2, N_3 \ldots . N_8 \end{bmatrix} \quad \begin{bmatrix} u_1 \\ u_2 \\ u_3 \\ \cdot \\ \cdot \\ \cdot \\ u_8 \end{bmatrix}$$

then first order differentials can be written in the form

$$\frac{\partial u}{\partial x} = \begin{bmatrix} \frac{\partial N_1}{\partial x}, & \frac{\partial N_2}{\partial x}, & \frac{\partial N_3}{\partial x}, \ldots . , & \frac{\partial N_8}{\partial x} \end{bmatrix} \quad \begin{bmatrix} u_1 \\ u_2 \\ u_3 \\ \cdot \\ \cdot \\ \cdot \\ u_8 \end{bmatrix}$$

since N is a function of spatial co-ordinates x,y.

9. ITERAT.

This is the main subroutine which calls the necessary subroutines for the evaluation and solution of the necessary matrix equations, transformation of boundary

conditions into a suitable form for incorporation into the matrix equations, output of results and check on the convergence tolerances when an iterative procedure is required.

10. FRONTS.

This subroutine formulates the global matrix, imposes the boundary conditions and solves the resulting matrix system of equations using a non-symmetric Frontal method. The required global matrix is assembled from contributions of element matrices as set up in the subroutine MATRIX.

11. MATRIX.

This subroutine forms the necessary relevant fluid matrix and corresponding right hand side vector.

12. TOLREL.

In this subroutine a check is made to ensure that the tolerance limits are met. If these are not met, updated values of the required coefficients are evaluated and the solution procedure is repeated.

13. MESGEN.

This subroutine is used for the calculation of space co-ordinates for each node in the mesh. The input for this is given in the form of space intervals in x and y directions.

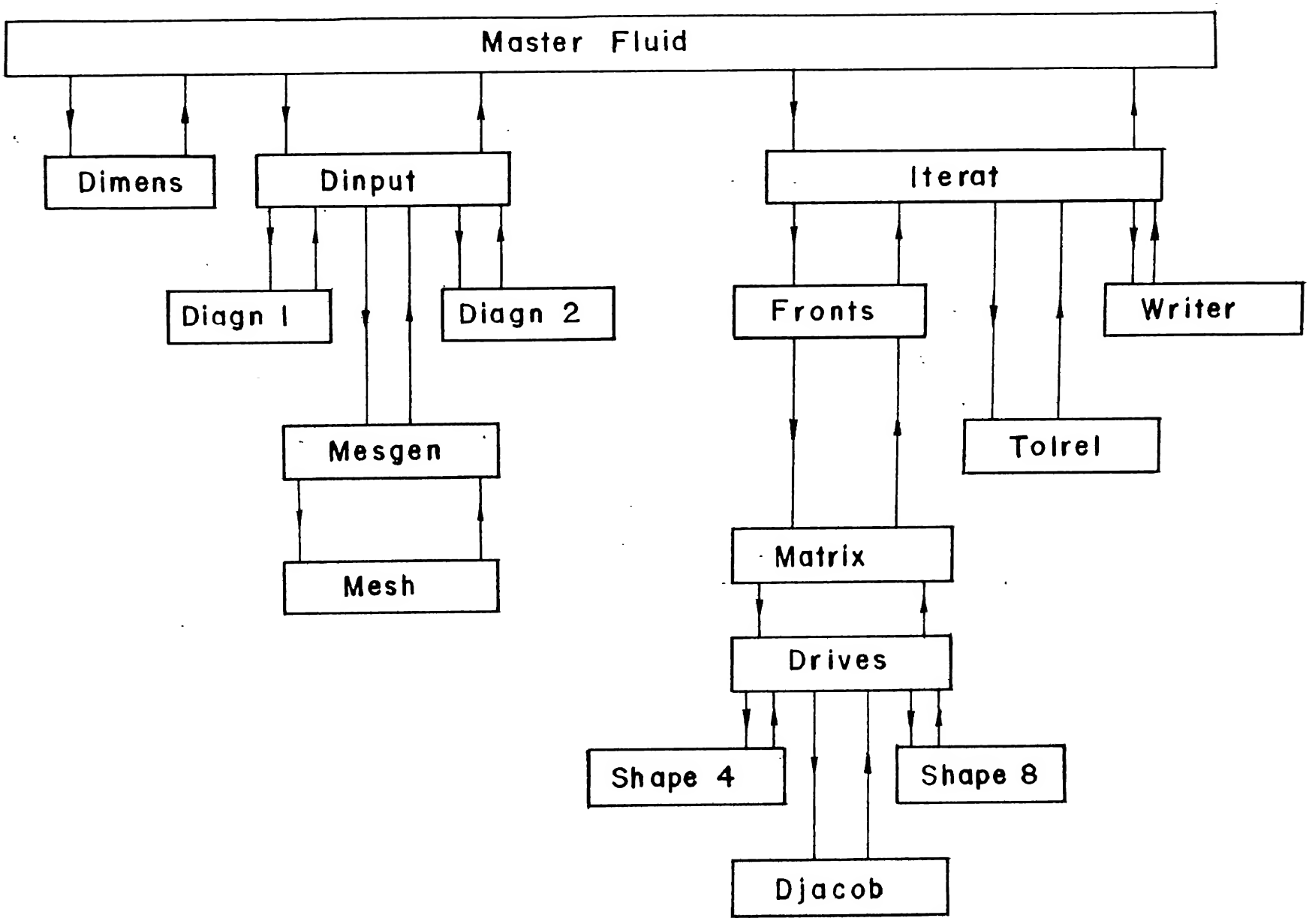


Fig. 4.1 General Program Structure

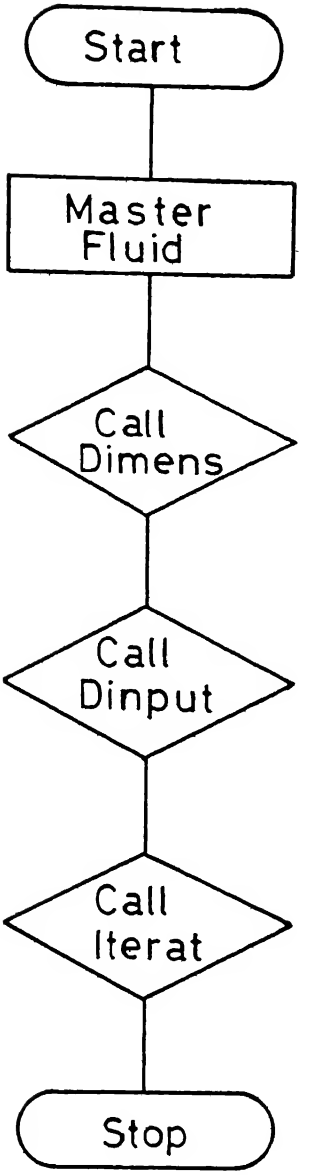


Fig.4.2 Flow-Chart

## 4.2 GENERAL STRUCTURE OF THE PROGRAM :

The general structure of the program alongwith various subroutines is shown in Figure 4.1. The flow-chart is shown in Figure 4.2. The working of the program consists of the following steps.

2. The subroutine DIMENS is called from the main program MASTER FLUID. This will set the dimensions of various arrays such as number of points, number of degrees of freedom in the program.

2. Subroutine DINPUT is called from the main program. This subroutine will collect information such as initial and boundary conditions of the problem. In DINPUT the program goes through the following steps.

   a. Subroutine MESGEN will be called from DINPUT for calculation of nodal co-ordinates and mesh-generation.

   b. Subroutines DIAGN1 and DIAGN2 are then called to check the data given through input, satisfy certain rules such as number of boundary conditions etc.

3. Subroutine DRIVES is called from the MATRIX This subroutine will calculate shape functions. Jacobians and global derivatives of the shape functions. The various steps in this are:

a. Subroutine SHAPE8 and SHAPE4 will be called to calculate the shape functions for each element.

b. Subroutine DTACOB will be called to calculate the derivatives of the shape functions with respect to the local co-ordinates.

c. Global derivatives of the above shape functions will be calculated.

d. Subroutine SHAPE4 will be called to calculate shape functions for 4 noded element.

e. Global derivatives of above shape functions will be calculated.

4. Subroutine ITERAT will be called to obtain the solution. The procedure is given below.

a. Subroutine FRONTS will be called to solve the governing equations. Here MATRIX subroutine is called for each element and these elemental matrices are assembled in subroutine FRONTS. The assembled matrix equations are solved and new values of the variables are obtained.

b. After calculating new values of variables, Subroutine TOLREL will be called to compare the difference between new and the old values of variables. If the

solution is within the required tolerance, control goes to subroutine WRITER to write the converged solution.

If the solution obtained is not within the required tolerance, new values of variables are relaxed using some relaxation factor and are taken as the new guesses for fresh iteration. The fresh iteration starts with a call to subroutine FRONTS.

## 4.3 SOLUTION OF ALGEBRAIC EQUATIONS :

As discussed in Chapter 3 the governing differential equations are converted into algebraic equations.

First of all, the calculation domain was divided into a number of elements and in each element certain number of points were selected as representatives of the pressure and velocity field inside the element. Here, eight points are chosen to represent velocity field and four points are chosen to represent pressure field inside the element.

When the governing differential equations are descretized for each element, a matrix of order 20 will be obtained whose solution will give values of variables

at the nodes . When such elemental matrices are assembled, the resulting global matrix in the present case becomes unsymmetric. Straight forward assembly of such elemental matrices requires a huge core memory in the computer when the number of elements increase. Hence, in the present case Frontal method is used to solve the matrix equations. The choice of the method has a significant bearing on computer storage requirement and execution time.

The overall solution technique consists of the following steps.

(i) Formation of elemental matrices (in Subroutine MATRIX)

(ii) Assembling into a global matrix.

(iii) Introduction of boundary conditions.

(iv) Reduction of the global fluid matrix using a Gaussian elimination technique.

(v) A back-substitution process.

First step in above sequence is already discussed. When the assembly of elemental matrices starts, then before the global matrix is completely assembled, certain equations can be eliminated using Gaussian elimination technique. This principle is used in the Frontal method.

As soon as all contributions from all the relevant elements to a particular nodal point are assembled then corresponding variables associated with that node can be eliminated. The complete matrix, is therefore, never assembled and the eliminated equations can be stored on a disc. The equations held in the core, with corresponding nodes and variables, are termed as the front and the number of unknown variables in front are termed as front width. Thus the order of the global matrix solved at the end will not be more than the specified front width. After the global matrix is solved, the eliminated equations stored on the disc can be solved using this solution.

# CHAPTER- V

# RESULTS AND DISCUSSION

## 5.1 GENERAL GUIDELINES :

As an example, the calculation domain divided into 64 elements is shown in Figure 3.3. The mesh is uniform in the Y-direction and non-uniform in the X-direction. Further, while dividing the mesh, care was taken to ensure that the aspect ratio of element does not exceed 8. This affects the accuracy of the solution.

Further, the ratio of the number of unknown velocities to the number of unknown pressures was atleast 2. If the ratio became less than two, it resulted in an ill-conditioned matrix. This was because the original equations contained second order derivatives of velocity and first order derivatives of pressure. To achieve this ratio, the element chosen was such that it had four pressure points (only corner points) and eight velocity points (corner points as well as mid-side points). Thus the mesh was designed to maintain this ratio (i.e. atleast 2 as stated above).

In the present case, the pressure could be specified only at the inlet and hence the mesh was finer here, so that larger number of pressures could be specified. The inlet velocity profile was assumed parabolic so that velocity was maximum at the centre of inlet and zero at the ends.

The results for various values of the parameters of a shell and tube heat exchanger are shown in Figures 5.1 through 5.7. Some explanation is given in each case. However, as no data were available to compare the results, the explanations are only qualitative. The results are used for validating the model rather than for predicting the performance. For all the cases presented here following data were used.

| | |
|---|---|
| Tube diameter | 20 mm |
| Tube pitch (square arrangement) | 25 mm |
| Ratio of shell length to shell diameter. | 2 |
| Ratio of inlet pipe diameter to shell diameter. | 0.1 |

Heat exchanger inlets and outlets were taken to be of the same size, though any combination could be tried.

The length of the heat exchanger and the center line velocity in the inlet pipe were used to non dimensionalize the equations. Hence the velocities calculated were non-dimensional.

For the heat exchanger tube-bank, the friction factors are given below(Salisbury, 1895).

(i) For flow along the tube bank, f= 0.02

(ii) For flow across the tube-bank, fr= 0.24.

The friction factors used here are applicable only when the tubes are arranged in a square pitch. It is to be noted that for calculating the pressure drops the equivalent diameter used is the hydraulic diameter which is defined as four times the free liquid-passage area divided by the liquid touched perimeter of the tubes.

The effect of changing the orientation of the heat exchanger and the Reynold's number is discussed in the following sections.

5.2 CASE-I :

Here, the fluid enters and leaves the heat exchanger in the direction of gravity i.e. gravity is in the positive Y-direction. The results are shown in Figures 5.1 through 5.5 . The value of Reynold's number was taken to be 1000.

Figure 5.1 shows velocity distributions along the line A-A (see Figure 3.3). The u-velocity is maximum after some distance from the inlet and then keeps on decreasing until it becomes zero at the wall. The v- velocity is maximum

at the inlet and then suddenly drops as the liquid expands after entering the heat exchanger. Then after a slight increase it also keeps on decreasing until it becomes zero at the wall.

Figure 5.2 shows velocity distributions along the line B-B (see Figure 3.3). This being the transverse section taken at the center of heat exchanger, u-velocity is maximum at the center and it reduces to zero at the walls. Further because of the position of inlet, the u-velocity at a particular point on B-B downstream of the point $O_B$ is greater than that at the corresponding point upstream of the point $O_B$. The v-velocity becomes maximum after some distance from the wall, then it reduces and remains almost constant in the central portion of the section. Near the other end of the wall (RS) it attains a slightly negative value before reaching zero at the wall.

Figure 5.3 shows velocity distributions along the line C-C which is a longitudinal section near the inlet of the heat exchanger (see Figure 3.3). After entering the heat exchanger, the liquid flows in all directions and hence u-velocity becomes negative for some portion along C-C. It then increases and remains almost constant for some length of the heat exchanger. It reaches zero at the wall after a slight

increase. This fluctuation is because of eddies near the wall. For v-velocity two distinct peaks are seen at equal distances on both sides of the center line of inlet. This is because of the sudden expansion of the liquid which makes it travel side-ways leaving the centre line. The right hand side peak is slightly larger which may be due to the fact that the outlet is on the right hand side of the section hence tendency of the liquid to travel more to the right. After second peak, v-velocity decreases and changes its direction several times before reaching a zero value due to the eddies prevailing near the wall.

Figure 5.4 shows velocity distribution along the line D-D (see Figure 3.3) which is a longitudinal section passing through the center of the heat exchanger. The velocity distribution is symmetric about the center. The u-velocity attains a maximum value near the center while the v-velocity reaches a minimum there.

Figure 5.5 is a plot of stream lines which shows an expected pattern. Stream lines having very low or high values of stream functions are closer to the walls of the heat exchanger. The eddies (not shown) are predominant near the wall $P_Q$(i.e. wall opposite to the outlet of the heat exchanger Further, there are almost no eddies near the outlet corner S.

The corner R opposite to the inlet wall has small eddies present (not shown).

## 5.3 CASE -II.

For this case, the orientation of heat exchanger was changed with respect to the direction of gravity i.e. the gravity acts in the positive X-direction. Figure 5.6 shows the nature of stream lines in this case for the same value of Reynold's number of 1000. It may be noted that there is a slight shift of stream lines in the X-direction as compared to the previous case. But it may be noted that there is a very little effect on the flow field because of change in the direction of gravity. Few runs were taken by changing the direction of gravity in negative Y and X-directions. It was noted that if the direction of gravity was changed from positive Y-direction to negative Y-direction, the flow-field showed almost insignificant change. On the other hand, when the direction of gravity was changed from positive X-direction to negative X-direction, there was a noticeable change in the flow-field. This may be explained as follows. The Y-force consists of resistance due to cross-flow over the tubes and gravity force if present in that direction. Now cross-flow resistance being much larger in

value dominates the gravity force. Hence even if the direction of gravity is changed, it has no significant effect on the flow-field. Whereas the resistance for axial flow over the tubes is much smaller in magnitude compared to the cross-flow resistance and it is comparable with the force of gravity, which explains the change in the flow-field with change in the direction of gravity from positive to negative X-direction.

## 5.4 CASE -III.

Here it was assumed that the gravity was in the positive Y-direction, but the value of Reynold's number was changed to 2000.

Figure 5.7 shows the velocity vectors in the calculation domain of the heat exchanger. It was noted that the nature of flow-field remained almost same except slight increase in the eddies inside. In this case the effect of gravity on the flow field was even more insignificant compared to the previous cases. It can be seen that as the Reynold's number increases the effect of gravity becomes even move insignificant.

98934

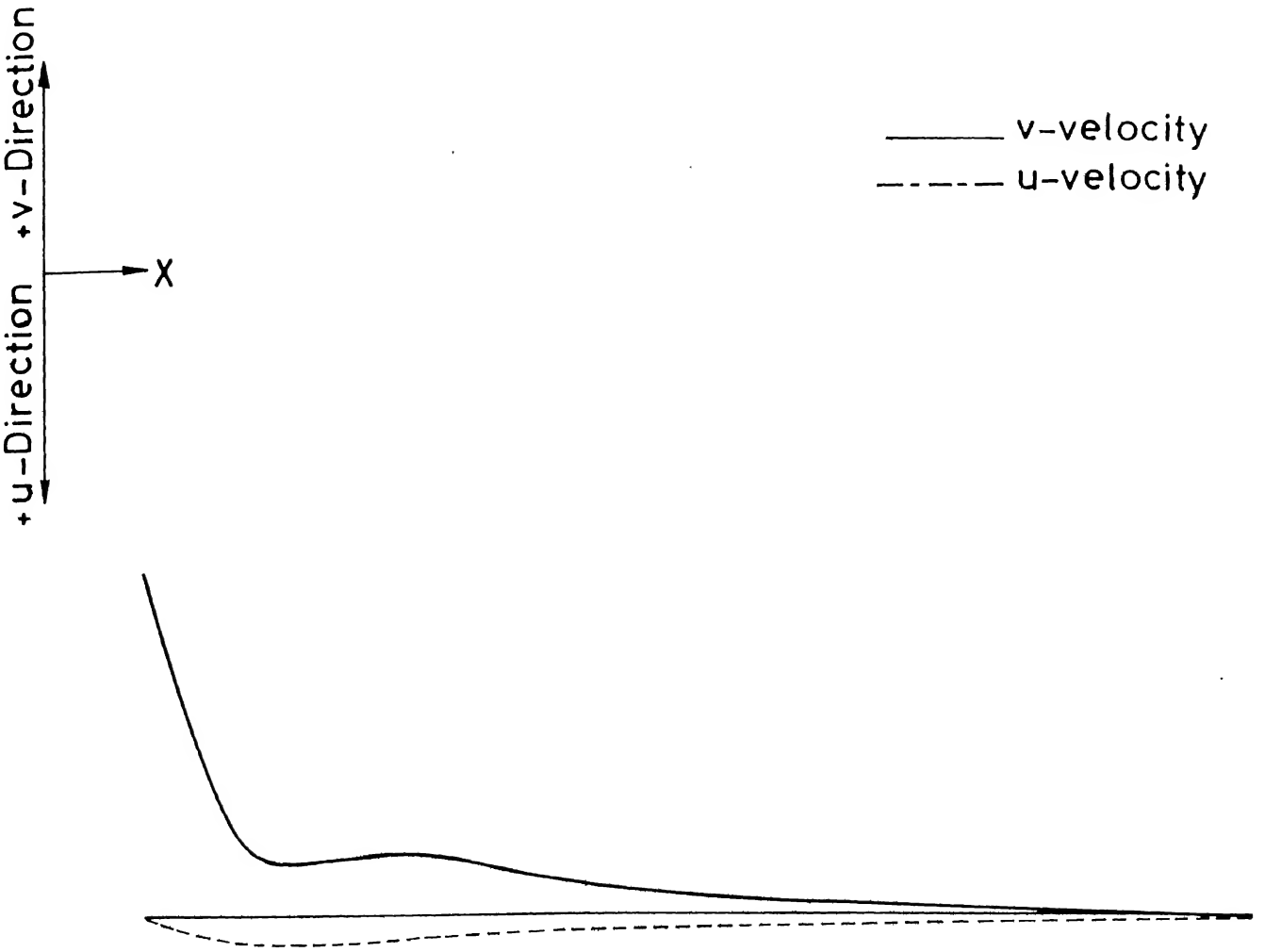


Figure 5.1 Velocity Distribution Along A-A

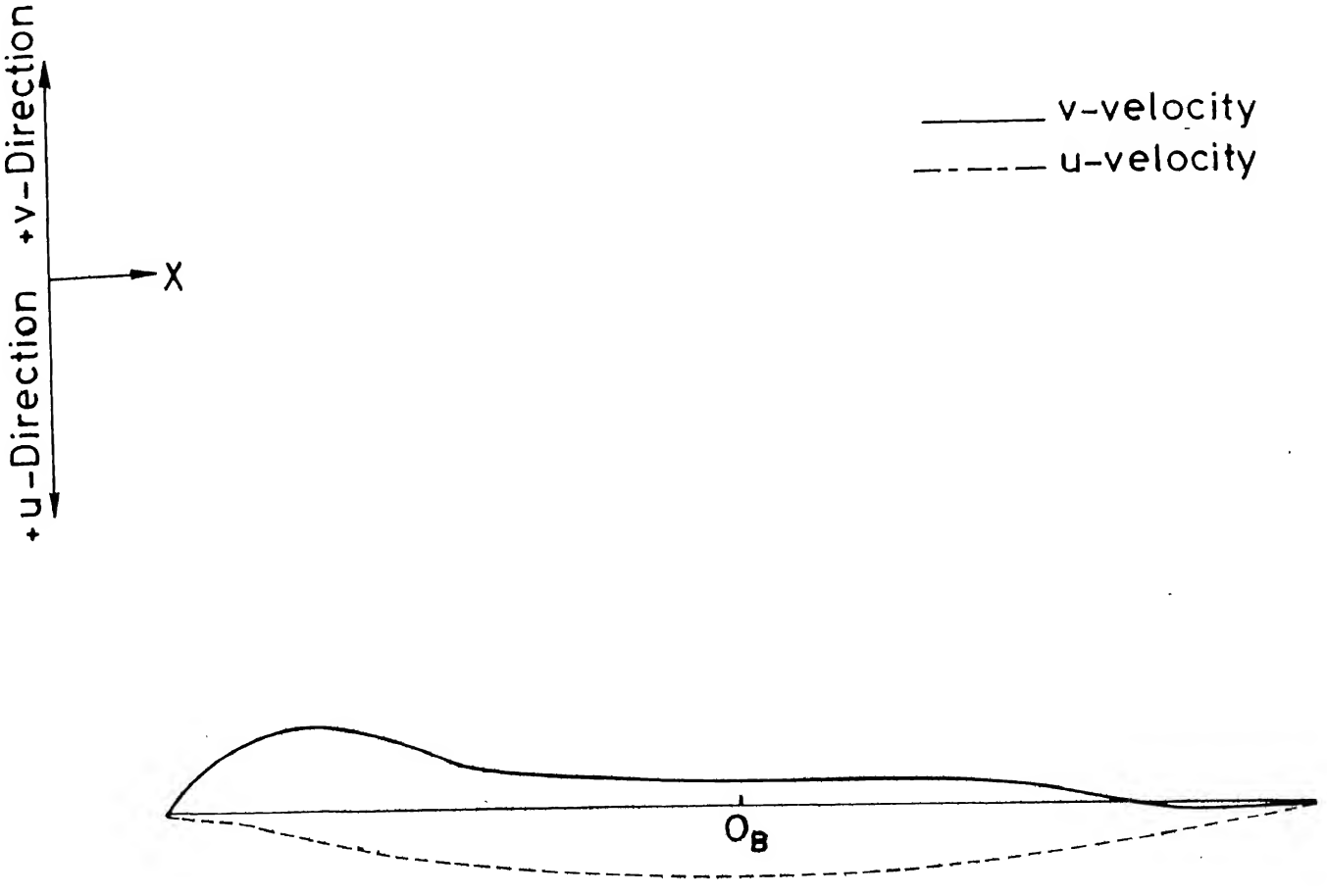


Figure 5.2 Velocity Distribution Along B-B

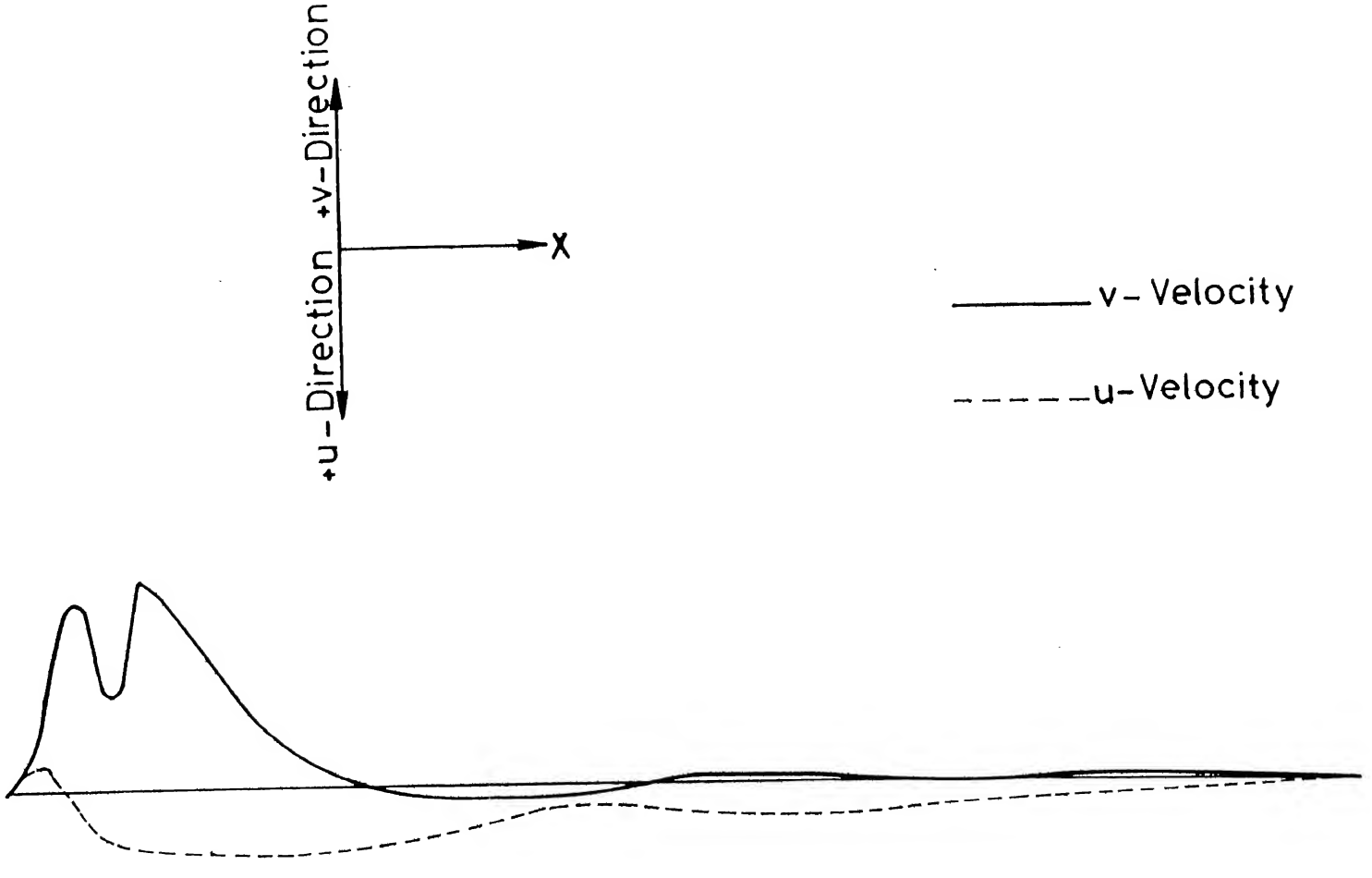


Figure 5·3 Velocity Distribution Along C - C

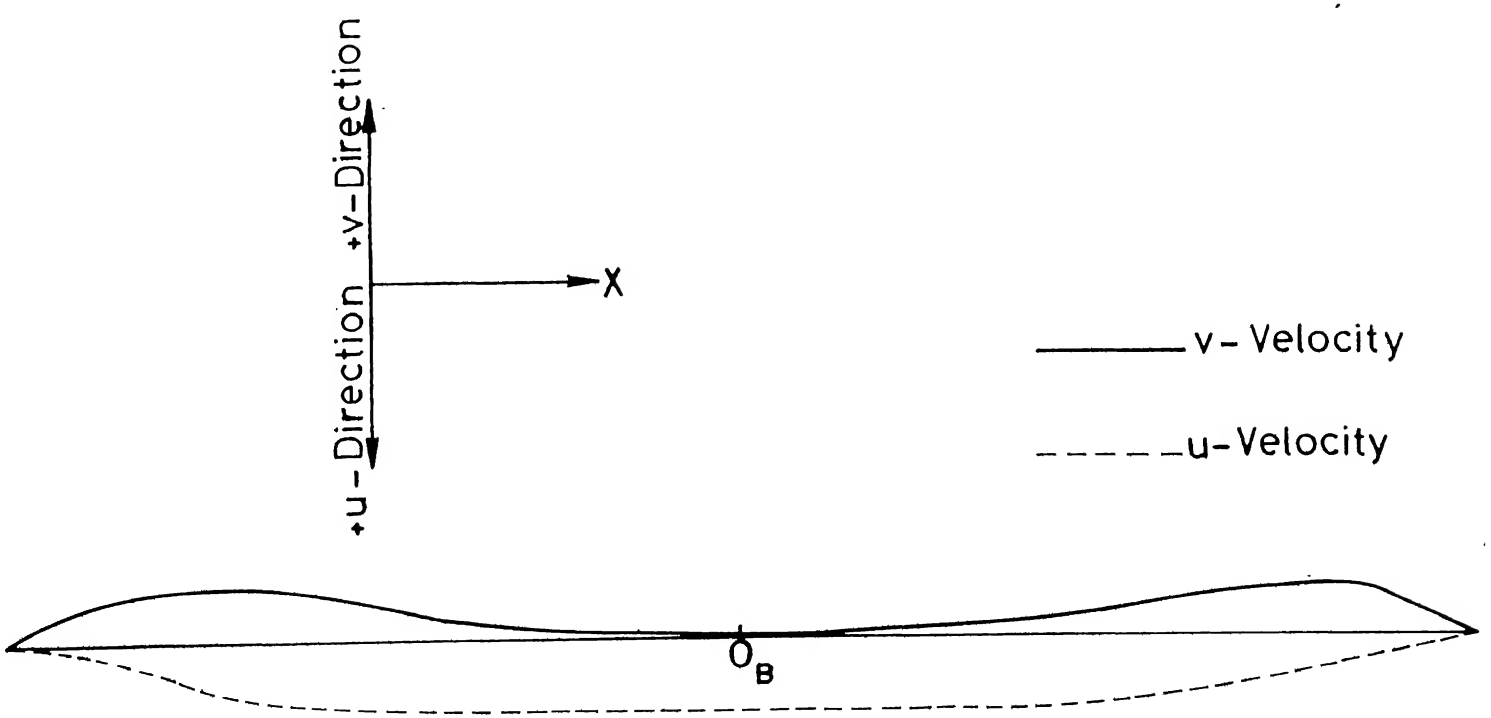


Figure 5·4 Velocity Distribution Along D-D

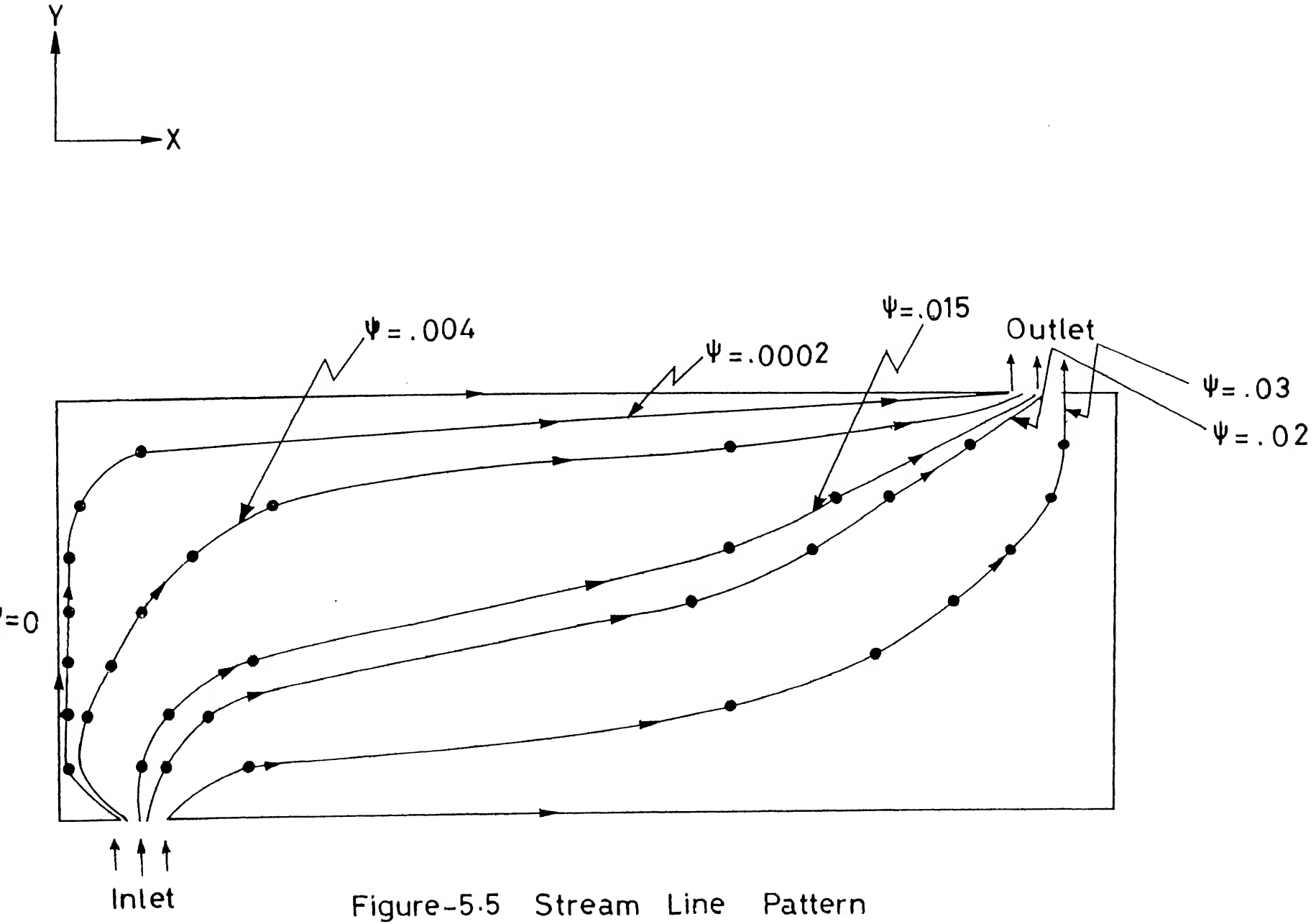


Figure-5.5 Stream Line Pattern

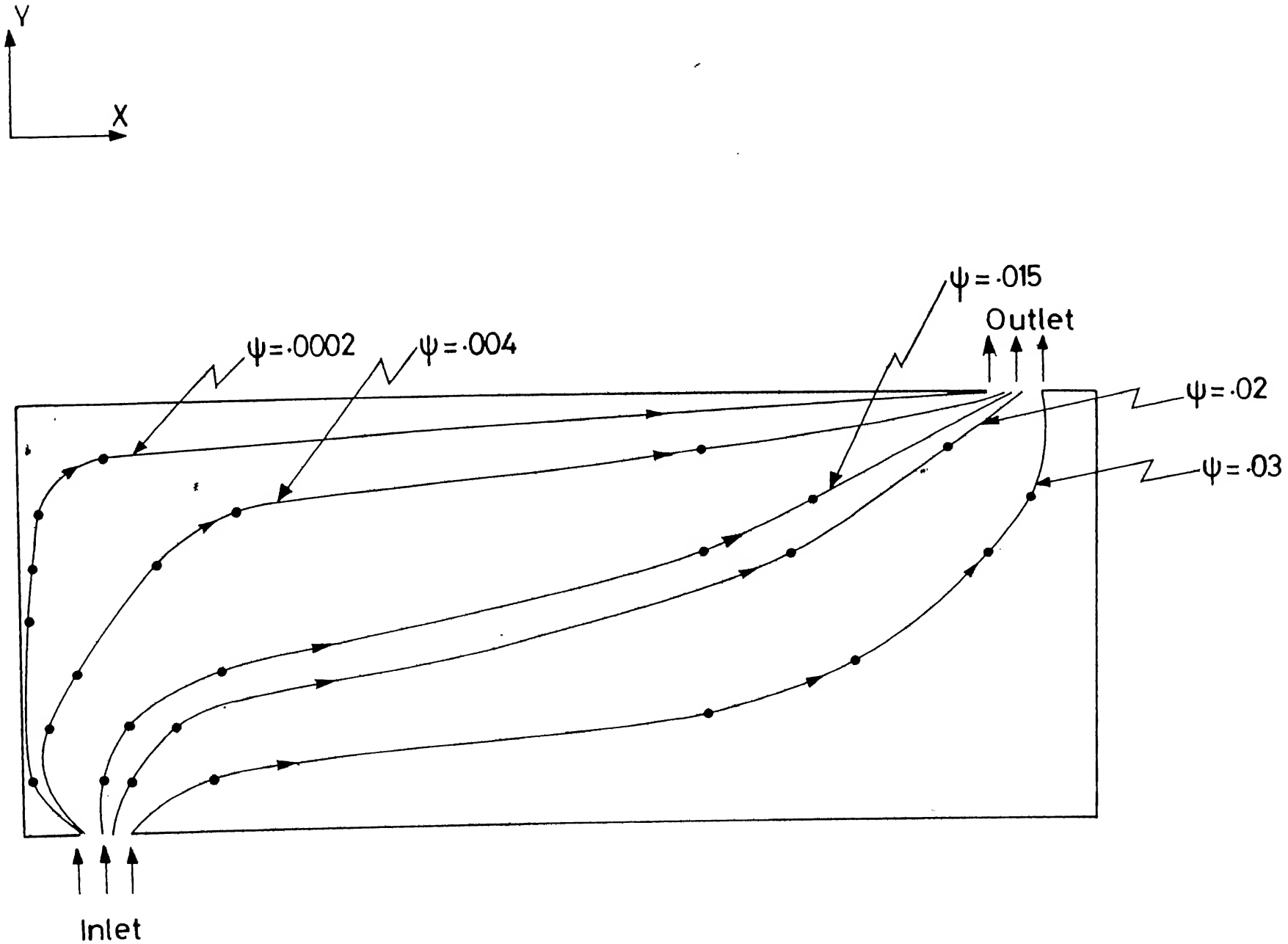


Figure 5·6 Stream Line Pattern

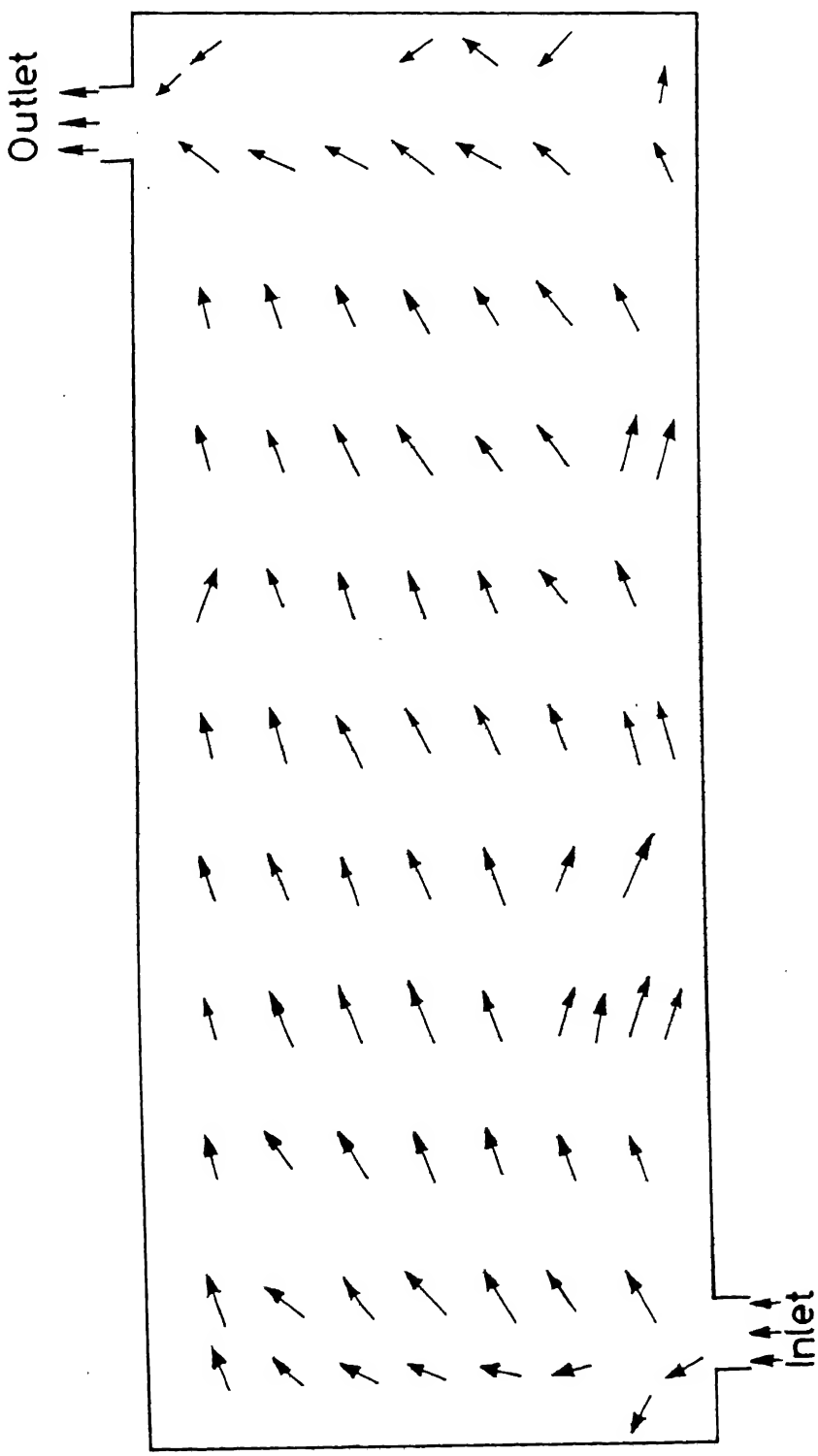


Figure 5.7 Velocity Vectors inside the Calculation Domain

## 5.5 CONCLUSIONS :

A FEM program was developed to solve the governing equations given in Chapter 3. The solution yielded the velocity distribution in a shell and tube heat exchanger without phase change. The computed results showed that for a given aspect ratio, the solution diverged for a particular value of Reynold's number. As the aspect ratio increased the limit of Reynold's number beyond which divergence occured was also increased. The program can be modified for use at high Reynold's number by incorporating eddy viscosity using the method given by Sha et. al. [1982].

Despite the difficulty of getting convergence at high Reynold's number as mentioned above, the results obtained in this thesis can be considered to be pretty realistic as the aspect ratio in general for shell and tube heat exchangers is much greater than two. The range is three to fifteen but a value of eight is generally used, [ Bhaskare, 1986] which will make it possible to get the converged solution at higher Reynold's number.

The objective of this work was to develop a code for flow-modeling of a shell and tube heat exchanger without phase change. Since this is the first attempt of two dimensional flow-modeling in a shell and tube heat exchanger using FEM, only the simpler cases of laminar flow at low

Reynold's number are dealt with in this thesis. There is a large scope for further work on this project as well as for refinements in the computation. The results are used only to validate the model as no data are available for comparison.

## 5.6 RECOMMENDATIONS FOR FUTURE WORK :

The code in the present version is limited to the two dimensional analysis of a shell and tube heat exchanger without phase change. The code developed has a flexibility to accomodate various changes easily. Since the method used is FEM, it can be extended easily to handle other geometries as well. For example, flow modeling for a plate type or spiral type heat exchanger can be easily done because of the fact that the element used in the code is parabolic, which can fit irregular boundaries. Further, the code can handle any type of boundary conditions i.e. variable specified boundary or the gradient specified boundary.

With little effort, energy equation can be added in the present code to use it for analysing thermal performance of a heat exchanger. The elemental matrix will be 28x28 in that case, with four degrees of freedom at the corner nodes and three degrees of freedom at the mid-side nodes.

For flow-modeling at very high values of Reynold's number say above 5000, a suitable turbulent viscosity model can be added to the present code which will update the viscosities at every node depending on the velocity at that node.

Further, the present code can be extended to three dimensional situations.

In case I and II, for a tolerance of $\pm$ 3%, 12 iteratic were required and the CPU time was 8 minutes. In case III, for the same tolerance limit 15 iterations were required and the CPU time was 10 minutes.

# BIBLIOGRAPHY


1. AbuRomia, M.M., Bosch, R.J., Jr., Cho, S.M., Dietz, D., and Jaisingh, G. ,"Flow Model Test Development of CRBRP Intermediate Heat Exchanger," ASME/IEEE Joint Power Generation Conference, Los Angeles, Calif., ASME Paper No. 77-JPGC-NE-10, Sept. 18-21, 1977.

2. AbuRomia, M.M., Chan, B.C., and Cho., S.M., "Flow Distribution Analysis in Nuclear Heat Exchanger with Applications to CRBRP- IHX," Proceedings of the 1976 Heat Transfer and Fluid Mechanics Institute, Stanford University Press, pp. 468-482, 1976.

3. Bhaskare', A.C., " An Expert System for the Design of Shell and Tube Heat Exchanger without Phase Change, " M.Tech. thesis, Dept. of Mechanical Engineering, I.I.T. Kanpur, India, August 1986.

4. Bhatnagar, R., "A Two fluid Model for the Digital Simulation of the Steam Generator Performance for the Analysis of Operational Transients," M.Tech. Thesis, Nuclear Engineering Dept. I.I.T. Kanpur, 1983.

5. Cook, R.D., " Concepts and Applications of Finite Element Analysis," John Wiley and Sons Inc., 1981.

6. Harlow, F.H., and Amsden, A.A., " A Numerical Fluid Dynamics calculation Method for All Flow Speeds," Journal of computational physics, vol. 8, pp. 197-213, 1976.

7. "Kent's Mechanical Engineering Handbook" , Power Volume, edited by Salisbury, J.K., John Wiley and Sons, Inc. 1895.

8. Oberjohn, W.J., Rice, J.G. and Patankar, S.V., "THEDA : A multi-dimensional steam Generator Analysis," AIChE 19th National Heat Transfer Conference, Orlando, Florida, July 27-30, 1980.

9. Patankar, S.V., and Spalding, D.B., "A calculation Procedure for Heat, Mass and Momentum Transfer in three Dimensional Parabolic Flows.", International Journal of Heat Mass Transfer, vol. 15, pp. 1787-1806, 1972.

10. Patankar, S.V., and Spalding, D.B., "A calculation procedure for the Transient and Steady-State-Behavior of Shell and Tube Heat Exchangers," Heat Exchangers Design and Theory Source book, edited by N.H. Afgan and E.V. Schlunder, pp. 155-176, McGraw-Hill, 1974.

11. Patankar S.V., "Numerical Heat Transfer and Fluid-Flow," Hemisphere Publishing Corporation, 1980.

12. Reddy, J.N., An Introduction to the Finite Element Method, McGraw Hill Publication, 1985.

13. Sha, W.T., "An Overview of Rod Bundle Thermal-Hydraulic Analysis," Argonne National Laboratory, Report No. NUREG/CR-1825, ANL-79-10, November 1980.

14. Sha, W.T., Yang, C.I., and Cho, S.M., "Multidimensional Numerical Modeling of Heat Exchangers," ASME Journal of Heat Transfer, Vol. 104, pp. 417-425, August 1982.

15. Zienkiewicz, O.C., "The Finite element Method", Tata McGraw Hill Publication, 1979.